Insight into incident photon to current conversion efficiency in chlorophylls

Samira Sabagh[1], Mohammad Izadyar[1,1], and Foroogh Arkan[1]

[1]Ferdowsi University of Mashhad

July 16, 2020

Abstract

Photovoltaic properties of the natural dyes of chlorophylls consist of Chl a, Chl b, Chl c2, Chl d, Phe a, Phe y and Mg-Phe a, were studied in the gas phases. The extension of the π-conjugated system, the substitution of the central Mg2+ and proper functional groups in the chlorophyll structures can amplify the charge transfer and photovoltaic performance. Chl a shows more favorable dynamics of charge transfer than other studied chlorophylls. Chl d, Phe a, Phe y and Mg-Phe a, have a greater rate of the exciton dissociation in comparison with Chl a, Chl b, and Chl c2 originated from a lower electronic chemical hardness, a lower exciton binding energy, and a bigger electron-hole radius. As a result, better efficiencies of the light-harvesting and energy conversion of the chlorophylls mainly appear in the Soret band. Finally, based on the energy conversion efficiency, Chl a, Phe a, and Mg-Phe a, are proposed as the best candidates for using in the dye-sensitized solar cells.

1 INTRODUCTION

Energy demand is dramatically increasing with the development of human society and the use of fossil fuels leads to serious environmental problems. [1,2] Solar energy is the most fundamental renewable energy source accessible today having clean and safe characteristics.[3] The photovoltaic cell is an electrical device that converts the light energy directly into electricity.[4] The first dye-sensitized solar cell (DSSC) was fabricated by O'Regan and Grätzel in 1991.[5]

A DSSC consists of a photosensitizer, an electrolyte, a titanium dioxide layer coated photoanode electrode, a counter electrode used as a cathode. [6] After photon absorption by a photosensitizer, an electron is excited from the highest occupied molecular orbital (HOMO) to the lowest unoccupied molecular orbital (LUMO). The excited electron enters the conduction band (CB) of TiO_2, which flows via the external load to the counter electrode to reduce the redox electrolyte (I^-/I_3^-), thereby regenerating the oxidized dye and completing the whole circuit.[7]

The molecular structure of the dye is one of the parameters that affect the photovoltaic performance of the DSSC, such as light-harvesting efficiency.[8] Natural dyes are abundant and safe material without environment threat[9] that cut down the high cost of the metal complex photosensitizers.[10] The ratio of the power conversion efficiency (PCE) to the cost of the dye in the natural-DSSCs (NDSSCs) is larger than that of ruthenium-based solar cells.[11] Natural dyes can be extracted from the flowers petals, leaves, roots and barks in the form of anthocyanin, flavonoid and chlorophyll pigments. [12-14]

Previous studies on the natural dyes of red-cabbage, curcumin and red perilla used in the solar cells showed that the energy conversion efficiency of the solar cell fabricated by using a mixture of red-cabbage and curcumin is higher than that of the solar cells using one kind of these dyes.[15] Also, the ratio of the PCE to the cost of the extracted cabbage is more than the synthetic ruthenium dye-based solar cell.[11] Moreover, to improve the spectroscopic properties, the ratio of cabbage to curcumin was changed. The abstained results showed that the maximum absorption at 430 and 550 nm are related to curcumin and red cabbage,

respectively. The greater efficiency of the solar cell was produced when the ratio of the extract of cabbage to the curcumin was 70:1.[15]

In the case of betalain derivatives including betanin, betaxanthin, and betanidin extracted from the red beetroot, electron transfer affects the energy conversion efficiency.[16] Among the betalain derivatives, betaxanthin represented a more efficient electron transfer, but due to the undesirable recombination of electron transfer to TiO_2 with the oxidized dye, light-harvesting efficiency (LHE) decreases.[16]

Some efficient push-pull systems, such as azo-bridged coumarin-purpurin based systems (CM1-CM7) were studied.[17] On the basis of the results, the substitution of the donor moiety (coumarin) and solvent affect the optoelectronic and photovoltaic properties of the D-π-D-π-A systems. Among these dyes, CM6 was preferred because of a proper band gap, polarizability, spectroscopic behavior and light-harvesting efficiency. Moreover, the interaction of the dyes with $(TiO_2)_6$ showed that these dyes are efficient photosensitizers for DSSCs.[17]

The influences of the chemical structure of the sensitizers on the photovoltaic properties were investigated. [17-20]For example, polypyridyl dyes based on Cr^{2+} and V^{3+} show better performance in comparison with ruthenium- and other scarce metal-based polypyridyl dyes due to the moderate LHE , high efficiencies of electron and hole injection, which make them promising alternatives to scarce Ru^{2+}metal ion.[18]

Also, theoretical insights into the effect of polycyclic aromatic hydrocarbons (PAHs) on monascus pigments (MPs) and as a photosensitizer for solar cells showed that the presentence of the PAHs reduces the electronic band gap and the electron injection efficiency of MPS.[19] Also, the absorption peaks of the MPs-fluorene, MPs-naphthalene, and MPs-anthracene appear in the visible region. The results confirm that these dyes can be used as a photosensitizer in the solar cells.

The flavylium compounds consist of anthocyanin pigments (callistephin, chrysanthemin, oenin, mytrillin) and anthocyanidin pigments (peonidin, petunidin) were investigated to identify their potential of application as the photosensitizer in the solar cell.[20]According to the obtained results, the peonidin dye is the preferred photosensitizer for DSSC because of good short-circuit current density, more ability to harvest light, the lower energy barrier for the electron injection, and favorable optic characteristics.[20]

Generally, natural dyes including chlorophyll, carotenoid, flavonoid, and anthocyanin are a relatively easy extract from the natural products in comparison whit the synthetic dyes.[21]Chlorophylls belong to the natural photosynthetic dye, which efficiently harvests the light and the photosynthesis.[22,23]Chlorophyll derivatives are applied as the photosensitizers in the DSSCs because of their ability to absorb blue and red light.

In this work, some metal-free and metal-based chlorophyll derivatives, such as **chlorophyll a** , **b** , **c2** and **d**(**Chl a** , **Chl b** , **Chl c2** , and **Chl d** , respectively) and pyropheophorbide-based chlorophylls, such as**Phe a** , **Phe y** and **Mg-Phe a** , are investigated. Since the optoelectronic characteristics of the photosensitizers are dependent on their rational design, molecular engineering is of great importance through the computational modeling of the NDSSCs.

Here, natural bond orbital (NBO) analysis, density functional theory (DFT) and time-dependent DFT (TD-DFT) methods are the main techniques to access the molecular orbital information, excited state properties, and charge transfer (CT) processes. Moreover, the behaviors of the exciton, the rate of free charge production and correlations of the energy conversion efficiency of the chlorophylls and DFT reactivity indices were evaluated through the computational approaches.

2 COMPUTATIONAL DETAILS

All calculations were performed by the Gaussian 09 program.[24] The ground and excited states of the chlorophyll-based dyes were investigated through DFT and TD-DFT methods at M062X/6-31G++(d) level of theory, respectively. Also, to obtain DFT reactivity indices, such as the electronic chemical hardness, η , the electronic chemical potential, μ , and the electrophilicity index, ω , Koopman's theorem, and NBO

analysis were used. The charge transfer distance, D_{CT} , and the overlap of e-h distribution, S , were obtained from the Multiwfn program.[25]

The performance of the NDSSCs was determined by the incident photon conversion to the current efficiency ($IPCE$) affected by the possibility of electron transfer between the frontier energy levels of the sensitizers and TiO_2/photosensitizer interface, which is theoretically obtained by Equation (1)[26]:

$$\Pi\Gamma E = \Lambda HE(\lambda).\Phi_{\iota\nu\vartheta.}\ \eta_{\varsigma o\lambda\lambda.} \quad (1)$$

where LHE is the light-harvesting efficiency, $_{coll}$ is the electron collection efficiency, and $_{\iota\nu\vartheta}$ is the net electron injection efficiency, which is related to Gibbs energy of electron injection, $\Delta\Gamma_{\iota\nu\vartheta.}$ The LHE of the sensitizer can be expressed by Equation (2)[27]:

$$LHE = 1 - 10^{-f} \quad (2)$$

where **f** is the oscillator strength of the dye molecule at the maximum absorption.

Electron injection from the excited states of the dye to the TiO_2 surface, $\Delta\Gamma_{\iota\nu\vartheta.}$, is given by Equation (3)[28]:

$$\Delta\Gamma_{\iota\nu\vartheta.} = E_{O\Xi,\delta\psi\epsilon*} - E_{CB(TiO_2)} \quad (3)$$

where $E_{CB(TiO_2)}$ is the conduction band energy of TiO_2, and $E_{OX,dye*}$ is the excited state oxidation potential of the photosensitizer. The driving force of the electron transfer from the photosensitizer toward semiconductor, eV_{OC} , is derived from Equation (4)[29]:

$$\mathrm{eV_{OC}} = E_{LUMO(dye)} - E_{CB(TiO_2)} \quad (4)$$

Exposed to radiation, an exciton as the Frenkel type is generated by a Coulomb energy between the electron and hole. The material-dependent constant, α , which shows the ratio of the Coulomb and exchange interactions between the excited electron and hole is evaluated through Equation (5)[30]:

$$E_B = \frac{(\alpha-1)^2\mu_x e^4 k^2}{2\alpha^2 tsh^2\varepsilon^2} \quad (5)$$

where E_B *(EBE)* is the electron-hole binding energy, ϵ_o is the vacuum permittivity, ε is the dielectric constant of the donor component, $\hbar$ is the reduced Planck's constant, $k = 9 \times 10^9 \mathrm{Nm^2C^{-2}}$, e is the electronic charge, and μ_ξ is the reduced mass of the exciton.

The rate of the photon absorption for a singlet excitation, R_a^S, is given by the transition matrix element and Fermi's golden rule, according to Equation (6)[31]:

$$R_a^S = \frac{4ke^2(E_{\mathrm{LUMO}} - E_{\mathrm{HOMO}})^3 {a_x}^2}{3c^3\varepsilon^{1.5}tsh^4} \quad (6)$$

where c is the light speed and a_x is the exciton radius. For the singlet excitons, a_x is given by Equation (7)[32]:

$$a_x = \frac{\alpha^2 \mu}{(\alpha-1)^2\mu_x} a_0 \quad (7)$$

where μ is the reduced mass of the electron in the hydrogen atom and a_o is the Bohr radius. The exciton dissociation rate, R_d , is obtained from Equation (8)[33]:

$$R_d = \frac{8\pi^2}{3tsh^3\varepsilon^2 E_B}\left[E^D_{\mathrm{LUMO}} - E^A_{\mathrm{CB}} - E_B\right]^2 (tsh\omega_\vartheta)\mu_x {a_x}^2 \quad (8)$$

where ω_{v} is the frequency of the incident phonon to the photosensitizer.

CT indices contain the corresponding effective CT distance, D_{CT} , and S as another quantity shows the overlap extent of electron-hole distribution. According to Equation (9), D_{CT} is defined as the distance between two barycenters (r_+ and r_-), which is an important factor to estimate the CT length[34]:

$$D_{\mathrm{CT}} = |r_+ - r_-| \quad (9)$$

Another quantity, which evaluates the overlap extent between the electron-hole,

is $S_{\pm}$ that is estimated according to Equation (10)[35]:

$$S_{\pm} = \int \sqrt{\frac{C_{+}(r)}{A_{+}}} \sqrt{\frac{C_{-}(r)}{A_{-}}} \mathrm{dr} (10)$$

where the normalization factor, A, is introduced so that the integrals of $C_{+}(\boldsymbol{r})$ and $C_{-}(\boldsymbol{r})$ are equal to the integrals of $\rho_{+}(\rho)$ and $\rho_{-}(\rho)$, based on total densities of the ground and excited states.

Polarizability character is the response of the dye to an applied electric field of the incident light. The polarizability tensors ($a_{\xi\xi}$, $a_{\xi\psi}$, $a_{\psi\psi}$, $a_{\xi\zeta}$, $a_{\psi\zeta}$, $a_{\zeta\zeta}$) are applied to evaluate the isotropic polarizability (Equation (11))[36]:

$$\alpha = \frac{1}{3}(\alpha_{\mathrm{xx}} + \alpha_{\mathrm{yy}} + \alpha_{\mathrm{zz}}) (11)$$

The excited-state lifetime, $\boldsymbol{\tau}$, is also evaluated as[37]:

$$\tau = \frac{1}{2\pi \upsilon_{\mathrm{max.}}} (12)$$

where $\boldsymbol{\tau}$ is the exciton lifetime and $\upsilon_{\mu a \xi}$ is the maximum frequency of the absorbed photon.

3 RESULTS AND DISCUSSION

3.1 Structural properties and charge transfer processes

The structures of the natural dyes based on chlorophyll consist of set **a** : **Chl a** , **Chl b** , **Chl c2** , and set **b** : **Chl d** , **Phe a** , **Phe y** , and **Mg-Phe a** , were optimized at M06-2X/6-31++G(d) level of theory. The optimized structures within natural sources and frontier energy levels are shown in Figure 1.

The frontier energy levels calculated by NBO analysis provides knowledge of the electronic transitions, which is important to evaluate the performance of the applied photosensitizers in the NDSSCs. According to Figure 1, the insertion of the central Mg^{2+} and various functional groups on the chlorophyll structure affects the energy of the frontier molecular orbitals. Considering Figure 1, the energy gaps between the lowest unoccupied molecular orbital of the photosensitizer and the CB of the semiconductor are more than 0.2 eV, which sufficient enough to transfer the electron. Also, the highest occupied molecular orbital levels of the chlorophylls are lower than the reduction potential of I^{-}/I_{3}^{-} electrolyte (-4.8 eV), which leads to an acceptable dye regeneration and suppress their electron recombination.

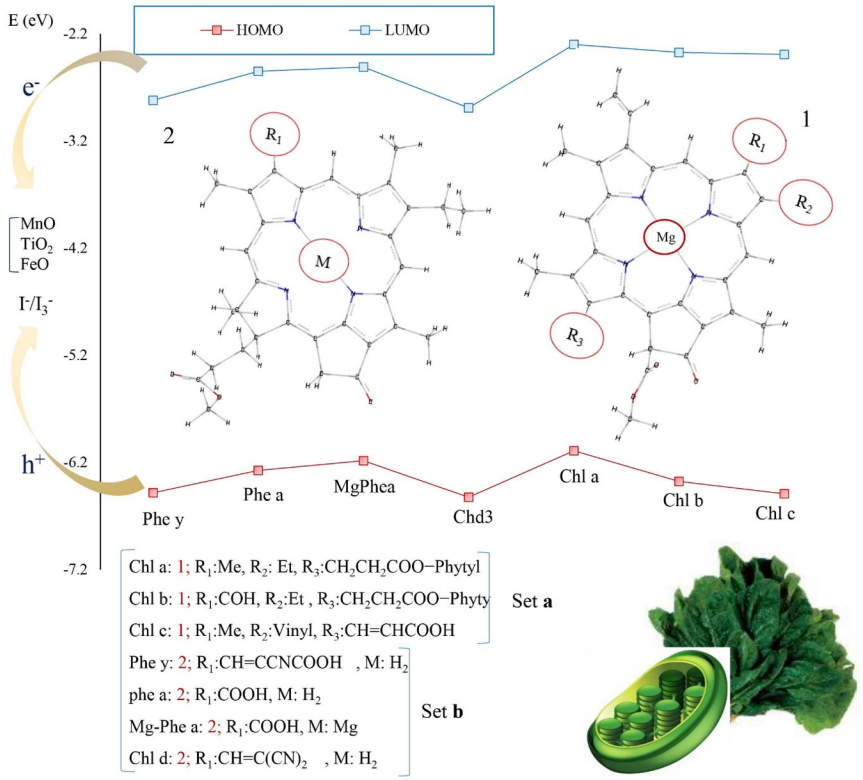

FIGURE 1 The energy diagram of the studied chlorophylls and the optimized structures within natural sources

To investigate the photovoltaic processes in the NDSSCs, DFT reactivity indices, electron driving force, eV_{OC} , the oxidation potential of the excited dyes,$E_{OX,dye*}$, the coupling constant of chlorophylls and TiO_2, V_{RP} , a change in the Gibbs energy of electron injection, $\Delta\Gamma_{\nu\vartheta.}$ and the exciton binding energy, EBE, were calculated and represented in Table 1. Moreover, the exciton radius, a_x , the rate of photon absorption for a singlet excitation,R_a, the rate of the exciton dissociation,R_d, light-harvesting efficiency, LHE , and the energy conversion efficiency, $IPCE$, the polarizability of the chlorophylls, α , the excited state lifetime, τ , and the charge transfer indices are reported in Table 2.

TABLE 1 The electronic chemical hardness, η, electronic chemical potential, μ, electrophilicity index, ω, electron driving fo

Dye
Phe a
Phe y
Mg-Phe a
Chl d
Chl a
Chl b
Chl c2

According to Table 1, the Gibbs energy of electron injection at the chlorophyll/TiO_2 interface has a negative character. Also, the electron driving force predominates to the exciton binding energy, EBE and the rate of the exciton dissociation,R_d , is faster than the exciton formation rate,R_a . These results show that the

primitive photovoltaic processes are efficiently occuring in the studied chlorophyll-based solar cells.

TABLE 2 Exciton *ra*dius (a_x; Å), the rate of a photon absorption (R_a; s^{-1}), rate of the exciton dissociation (R_d; s^{-1}), light-

Dye
Phe a
Phe y
Mg-Phe a
Chl d
Chl a
Chl b
Chl c2

Figure 2 shows the correlation of the reactivity indices and photovoltaics parameters. **Chl a** , **Chl b** , and**Chl c2** have a lower electrophilicity, which leads to a decrease in their tendency of electron reception and enhancement of the electron migration toward TiO_2. Set **a** of the chlorophylls also has greater polarizability in the case of the applied electric field of the incident radiation. Moreover, a decrease in the electronic chemical potential increases the ability of the chlorophylls to drive the electronic charges.

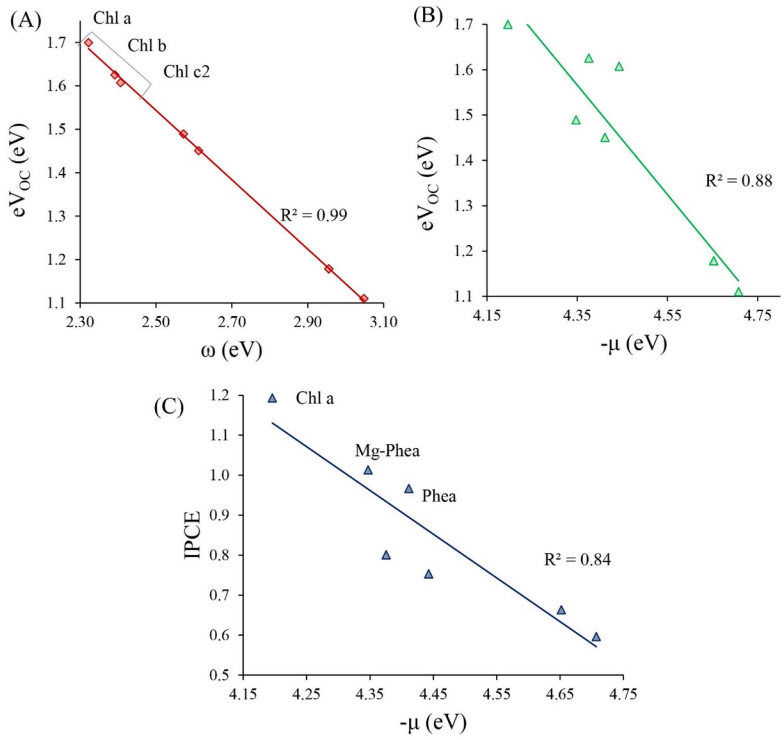

A decrease in the electronic chemical potential develops the light-harvesting efficiency and the ability of the electricity production in the natural dyes (Figure 2C). **Chl a** , **Chl b** , and **Chl c2** having a central Mg^{2+} show better intermolecular charge transfer (ICT). On the other hands, the existence of a longer π-conjugated system and resonance amplification in the chlorophyll structures improve their photovoltaic performance. In

addition, Table 2 shows that softer chlorophyll derivatives, such as**Chl d** and **Phe y** are better candidates for coupling with TiO_2. A greater lifetime of the excited state and bigger coupling-constant of **Chl d** and **Phe y** is according to weaker charge recombination.

FIGURE 2 Linear correlations of the electron driving force vs. the electrophilicity (A) and electronic chemical potential of the chlorophylls (B). The correlation of energy conversion efficiency andμ (C)

In Figure 3, the changes of the energy barrier of the electron transfer at the chlorophyll/TiO_2 interfaces and energy conversion efficiency of the NDSS show a harmony. According to these trends,$IPCE$ is dependent on the $[?]G_{inj}$ greater than LHE . Moreover, **Chl a** and **Mg-Phe a**chlorophylls have a lower excited state oxidation potential,$E_{OX(dye*)}$, and greater negative character of the Gibbs energy of electron injection, which increases the final efficiency of the NDSSCs ($IPCE$).

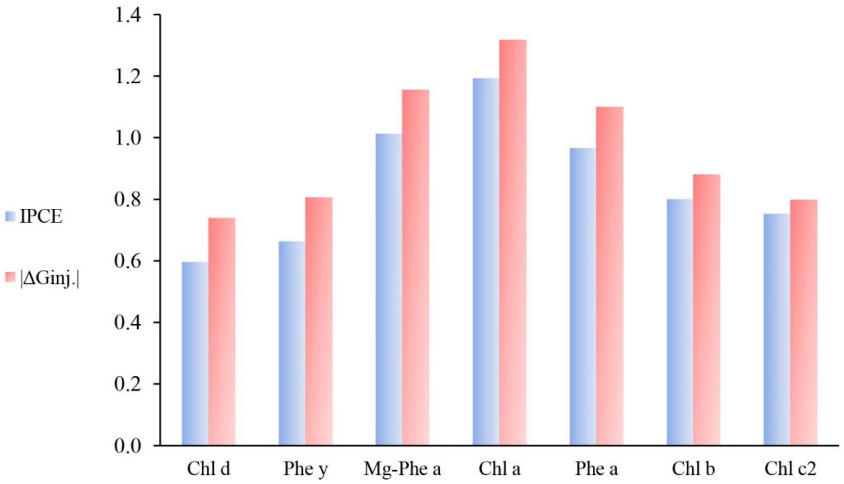

FIGURE 3 Theoretical changes of the Gibbs energy of the electron injection and the energy conversion efficiency

The rate of the exciton dissociation in the studied chlorophylls,R_d , are affected by the band gap (Figure 4A) and the exciton binding energy (Figure 4B). Also, the exciton binding energy and R_d are related to the exciton radius, and the electronic chemical hardness of the chlorophylls, respectively (Figure 4C and 4D).

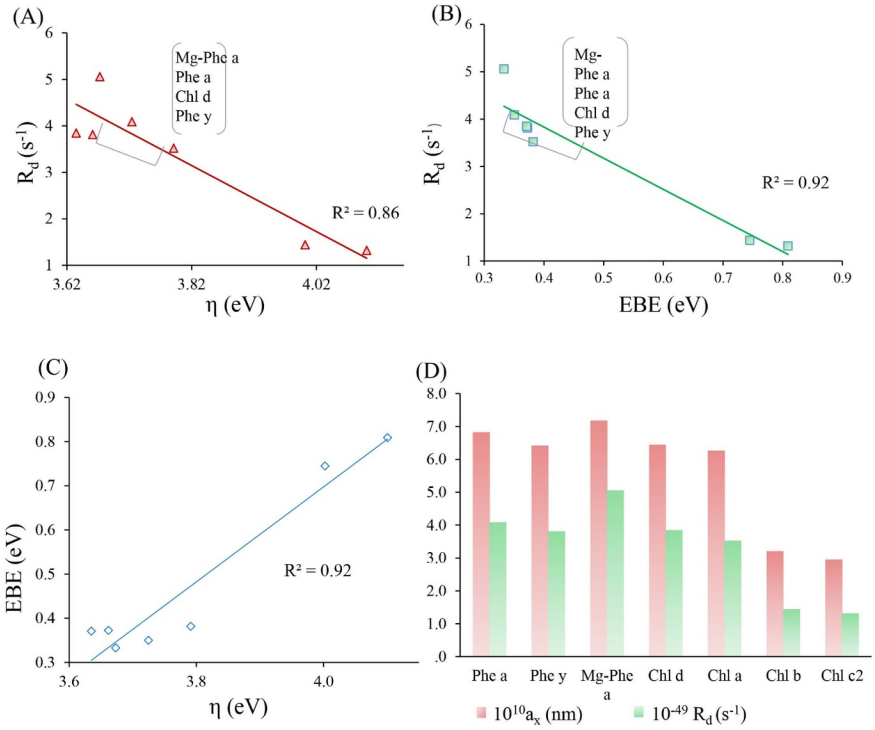

FIGURE 4 The rate of the exciton dissociation as a function of the band gap (A) and the exciton binding energy (B). EBE andR_d change vs the electronic chemical hardness of the chlorophylls (C) and exciton radius (D)

According to Figure 4, free charges are produced faster in set**b** (**Chl d** , **Phe a** , **Phe y** , and**Mg-Phe a**) in comparison with set **a** (**Chl a** ,**Chl b** , and **Chl c2**) originated from a greater softness of the materials and an easier separation of the electron-hole in set**b** . Such an easier separation of the exciton is due to a bigger radius and lower binding energy of the electron-hole.

3.2. UV-Visible spectroscopy of the studied chlorophylls

The simulated UV-Vis spectra of the studied chlorophylls within the frontier molecular orbital transition configuration contributed to the maximum absorption peaks are displayed in Figure 6, and the corresponding data are represented in Table 3.

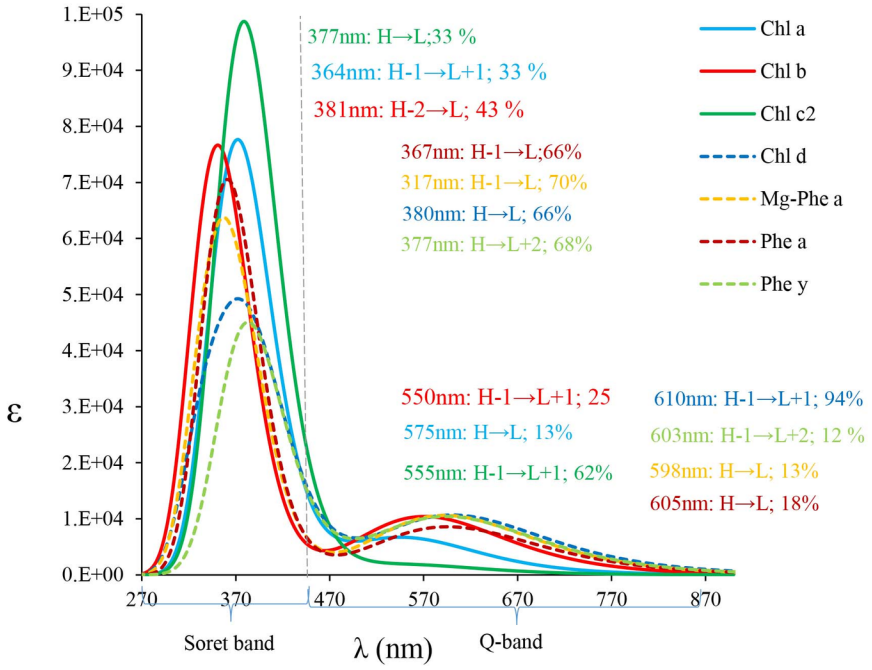

FIGURE 5 The simulated absorption spectra of the studied chlorophylls within the frontier molecular orbital transition configuration contributed to the maximum absorption peaks calculated at the TD-DFT/M062X/6-31++G(d) level of theory

TABLE 3 Theoretical vertical excited energies, $E_{0\text{-}0}$, oscillating strength, f, the maximum absorption wavelength (nm), light

Dye
Phe y
Phe a
Mg-Phe a
Chl d
Chl a
Chl b

TABLE 3 Theoretical vertical excited energies, $E_{0\text{-}0}$, oscillating strength, f, the maximum absorption wavelength (nm), light

Chl c2

The studied chlorophylls show two main absorption peaks consist of the Soret band in 300 to 450 nm and Q band with a wavelength >450 nm. In the Soret band, chlorophyll **c2** has the most intense absorption peak and the highest red shift in the absorption wavelength. In the Q-band, **Chl d** and **Phe y** show more proper spectroscopic properties originated from a higher probability of the electron transfer between their frontier molecular, tighter band gap (Figure 5 and Table 2), lower overlap of the electron-hole distribution, S , and a longer charge transfer distance,D_{CT} .

LHE changes as a function of the electric transition dipole moment, $r_{k,k'}$, are shown in Figure 6A. This Figure shows that the chlorophylls in set **a,** having a higher electric dipole moment, show a more probable charge transfer between the molecular orbitals. According to quantum mechanics, a higher$r_{k,k/}$ means greater oscillating strength and intrinsic transition probability, which can increase the ability of the chlorophylls to harvest the light.

To evaluate the NDSSCs efficiencies, light-harvesting and energy conversion efficiency of the chlorophylls efficiency were illustrated as the function of the maximum absorption wavelength (Figures 6B and 7, respectively). **Chl a** , **Chl b** , and **Chl c2** have a greater ability of the light-harvesting and electron transfer between the molecular orbitals (Figure 6B).

According to the results, a higher energy conversion efficiency is mainly appeared in the Soret band, which is according to the maximum oscillating strength. Finally, the dyes based on **Chl a** ,**Phe a** and **Mg-Phe a** are the preferred dyes because of the lower energy barrier of the charge transfer and higher *IPCE*(Figure 7).

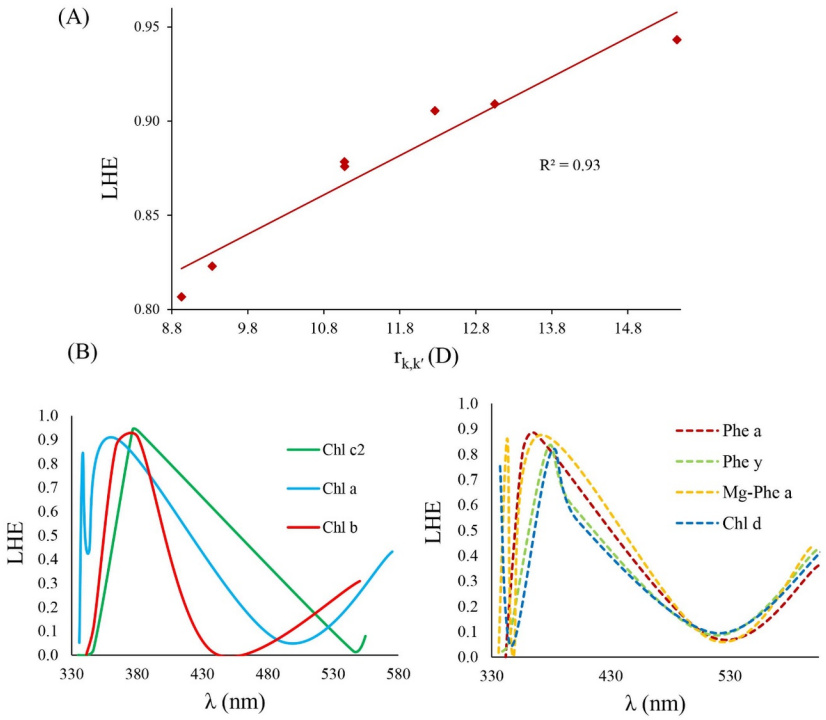

FIGURE 6 The correlation of *LHE* as a function of $r_{k,k}$ (A). *LHE* values of the chlorophylls according to the maximum absorption wavelength (B)

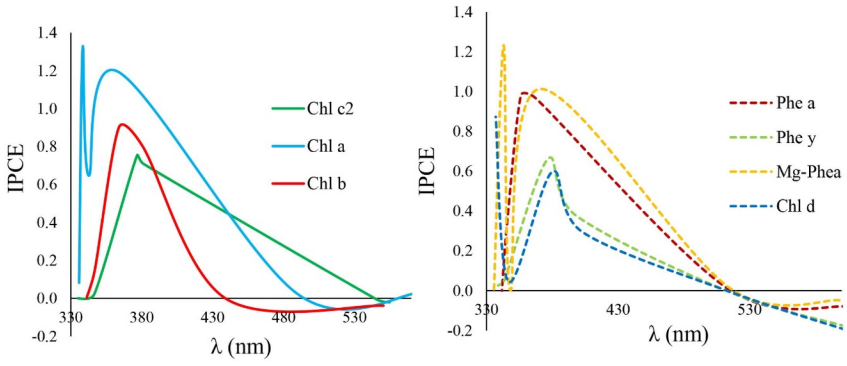

FIGURE 7 Theoretical behavior the *IPCE* values of the chlorophylls against to maximum absorption wavelength

According to the electronic density distribution of the frontier molecular orbitals (Figure 8), structural modification of the chlorophylls does not affect the HOMO-LUMO distribution property. Because they are mainly distributed in the central ring of the chlorophylls. The energy conversion efficiency is mainly affected by the dynamics of the charge transfer, such as the Gibbs energy of the electron injection from the chlorophylls to TiO_2.

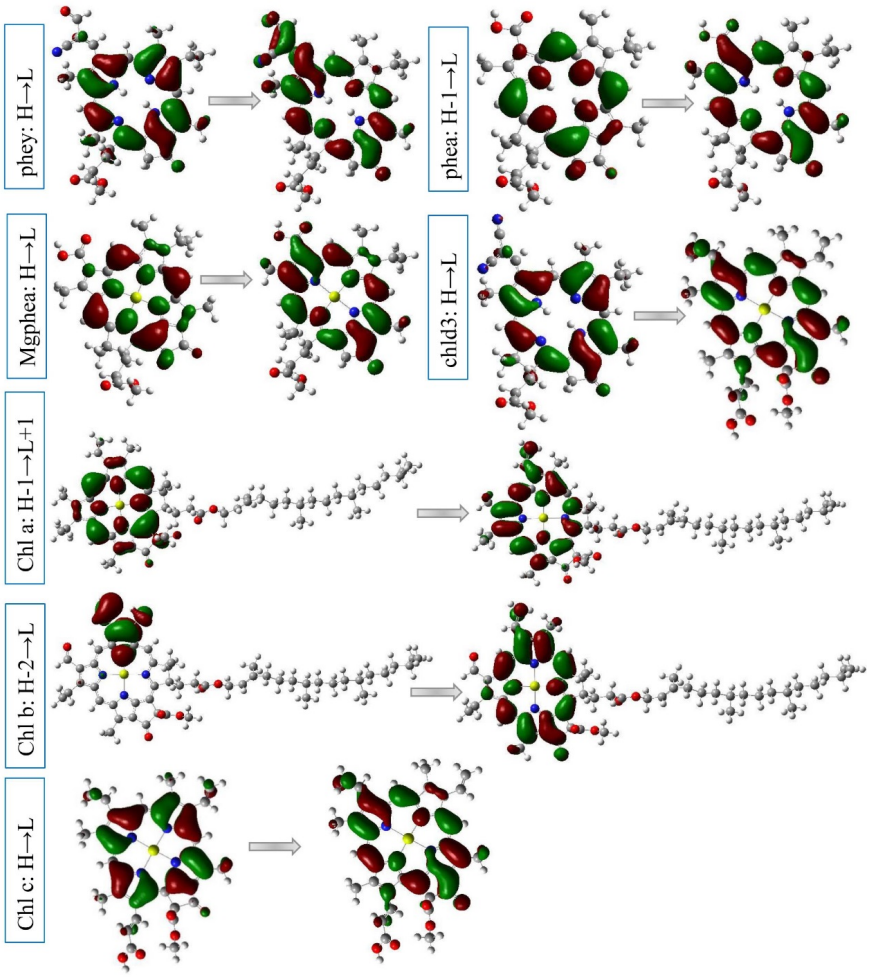

FIGURE 8 Electron density distribution of the frontier MOs in the studied chlorophylls

4 CONCLUSION

In this research, the feasibility of using of chlorophylls **a** ,**b** , **c2** , **d,** and the pyropheophorbide-based chlorophylls **(Phe a** , **Phe y** , and **Mg-Phe a**) in the NDSSCs was performed, dynamically and kinetically. The insertion of Mg^{2+} and various functional groups in the chlorophyll structure affect the energy levels of the corresponding molecular orbitals, DFT reactivity indices, and the photovoltaic processes. The studied chlorophylls can be considered as the efficient photosensitizers in the NDSSCs due to negative value of the Gibbs energy of the electron injection, the predominance of the electron driving force, eV_{OC} , to the exciton binding energy, EBE, and their ability in the generation of free charges. Based on the results, a decrease in the electrophilicity index and the electronic chemical potential of the chlorophylls increases the electron driving force and the energy conversion efficiency. Also, **Chl a** has the lowest energy barrier of the charge transfer at the dye/TiO_2interface and the highest *IPCE* . Meanwhile, **Chl d** ,**Phe a** , **Phe y** , and **Mg-Phe**

a represent more favorable kinetic behavior in the charge transfer process because of a tighter band gap and a lower exciton binding energy. In the Soret and Q bands, chlorophyll **c2** , **Chl d** (and **Phe y**) derivatives have preferred spectroscopic properties, respectively. On the basis of obtained results, **Chl a** , **Phe a** , and**Mg-Phe a** have a higher capacity to produce the electricity, which makes them the best candidate for NDSSCs.

ACKNOWLEDGMENTS

Research Council of the Ferdowsi University of Mashhad is gratefully acknowledged for supporting this project (3/48345).

RFERENCES

1. Y. Shang, S. Hao, C. Yang, G. Chen, *Nanomaterials***2015,** 5, 1782
2. M. Kutraleeswaran, M. Venkatachalam, M. Saroja,; P. Gowthaman, S. Shankar, *J. Adv. Res. Appl. Sci* . **2017,** 4, 26.
3. S. Galliano, F. Bella, C. Gerbaldi, M. Falco, G. Viscardi, M. Grätzel, C. Barolo, *Energy Technol.* **2017** , 5, 300.
4. G. Calogero, J. H. Yum, A. Sinopoli, G. Di Marco, M. Gratzel, M. K. Nazeeruddin. *Sol. Energy.* **2012,** 86, 1563.
5. B. O'regan, M. Gratzel, *Nature* **1991** , 353, 737.
6. A. Imbrogno, R. Pandiyan, A. Macario, A. Bonanno, M. A. El Khakani, *IEEE J. Photovolt* . **2019**
7. K. Fan, J. Yu, W. Ho, *Mater. Horizons.* **2017** , 4, 319.
8. F. De Angelis, S. Fantacci, E. Mosconi, M. K. Nazeeruddin, M. Gratzel,*J. Phys. Chem. C* **2011,** 115, 8825
9. G. Richhariya, A. Kumar, P. Tekasakul, B. Gupta, *Renew. Sust. Energ. Rev.* **2017** , 69, 705.
10. M. Kutraleeswaran, M. Venkatachalam, M. Saroja, P. Gowthaman, S. Shankar, *J. Adv. Res. Appl. Sci* . **2017** , 4, 26.
11. N. T. R. N. Kumara, A. Lim, C. M. Lim, M. I. Petra, P. Ekanayake, *Renew. Sust. Energ. Rev* . **2017** , 78, 301.
12. N. Prabavathy, S. Shalini, R. Balasundaraprabhu, D. Velauthapillai, S. Prasanna, N. Muthukumarasamy, *Int. J. Energy Res.***2017** , 41, 1372.
13. M. R. Narayan, *Renew. Sust. Energ. Rev.* **2012** , 16, 208.
14. M. Shahid, F. Mohammad, *J. Clean. Prod.* **2013** ,*53* , 310.
15. S. Furukawa, H. Iino, T. Iwamoto, K. Kukita, S. Yamauchi, *Thin solid films* **2009** , 518, 526.
16. C. I. Oprea, A. Dumbravă, I. Enache, A. Georgescu, M. A. Gîrţu,*J. Photochem. Photobiol.* **2012** , 240, 5.
17. T. Manzoor, S. Niaz, A. H. Pandith, *Int. J. Quantum Chem.***2019** , 117, e25979.
18. A. Sen, A. Groß, *Int. J. Quantum Chem* . **2019** , 119, e25963.
19. A. M. Khudhair, F. N. Ajeel, M. H. Mohammed, *Microelectron. Eng.* **2019** , 212, 21-26.
20. A. Sinopoli, G. Caloger, A. Bartolotta, *Food Chem.* **2019,** 297, 124898.
21. S. Shalini, S. Prasanna, T. K. Mallick, S. *Renew. Sust. Energ. Rev.* **2015** , 51, 1306.
22. Y. Li, M. Chen, *Funct. Plant Biol.* **2015** , 42, 493.
23. M. J. Garcia-Salinas, M. J. Ariza, *Appl. Sci.* **2019** , 9, 2515.
24. M. J. Frisch, G. W. Trucks, H. B. Schlegel, G. E. Scuseria, M. A. Robb, J. R. Cheeseman, G. Scalmani, V. Barone, B. Mennucci, G. A. Petersson, H. Nakatsuji, M. Caricato, X. Li, H. P. Hratchian, A. F. Izmaylov, J. Bloino, G. Zheng, J. L. Sonnenberg, M. Hada, M. Ehara, K. Toyota, R. Fukuda, J. Hasegawa, M. Ishida, T. Nakajima, Y. Honda, O. Kitao, H. Nakai, T. Vreven, J. A. Montgomery Jr.., J. E. Peralta, F. Ogliaro, M. Bearpark, J. J. Heyd, E. Brothers, K. N. Kudin, V. N. Staroverov, R. Kobayashi, J. Normand, K. Raghavachari, A. Rendell, A. Rendell, J. C. Burant, S. S. Iyengar, J. Tomasi, M. Cossi, N. Rega, J. M. Millam, M. Klene, J. E. Knox, J. B. Cross, V. Bakken, C. Adamo, J. Jaramillo, R. Gomperts, R. E. Stratmann, O. Yazyev, A. J. Austin, R. Cammi, C. Pomelli, J. W. Ochterski, R. L. Martin, K. Morokuma, V. G. Zakrzewski, G. A. Voth, P. Salvador, J. J. Dannenberg,

S. Dapprich, A. D. Daniels, O. Farkas, J. B. Foresman, J. V. Ortiz, J. Cioslowski, D. J. Fox, Gaussian 09, revision A02, Gaussian, Inc., Wallingford, CT**2009** .
25. T. Lu, F. Chen, *J. Comput. Chem.* **2012** , 33, 580.
26. F. Barati-darband, M. Izadyar, F. Arkan, *The J. Phys. Chem. A* **2019** , 123, 2831-2842.
27. Y. C. Li, Y. Q. Feng, Y. T. Wang, C. C. Fan, X. J. Liu, X. G. Li, B. Zhang, *Int. J. Quantum Chem.* **2014** , 114, 222.
28. F. Barati-Darband, M. Izadyar, F. Arkan, *J. Phys. Chem. C***2018** , 122, 23968.
29. F. Arkan, M. Izadyar, *Sol. Energy* . **2019** , 194, 51-60.
30. A. Arunkumar, P. M. Anbarasan, *J. Electron. Mater.* **2019** , 48, 1522.
31. S. B. Novir, S. M. Hashemianzadeh, *Current Appl. Phys.***2014,** 14, 1401.
32. S. Sabagh, M. Izadyar, F. Arkan, *Int. J. Quantum Chem.***2020** , 120, e26171.
33. M. R. Narayan, J. Singh, *J. Appl. Phys.* **2013** , 114, 154515.
34. M. K. Gish, N. A. Pace, G. Rumbles, J. C. Johnson, *J. Phys. Chem. C* **2019** ,123, 3923.
35. L. N. Yang, L. G. Lin, A. L. Meng, Z. J. Li, *J. Photochem. Photobiol.* **2019** , 369, 25-33.
36. T. Le Bahers, C. Adamo, I. Ciofini, *J. Chem. Theory Comput.***2011** , 7, 2498.
37. A. S. Shalabi, S. Abdel Aal, A. M. El Mahdy, *Mol. Simul.***2013** , 39, 689.
38. Y. Dou, F. Wu, L. Fang, G. Liu, C. Mao, K. Wan, M. Zhou, *J. Power Sources.* **2016,** 307, 1.